Studying a Two-Stage Robust Optimization Maximal Load Delivery (MLD) Framework on a Large-Scale Distribution System

Irfan Ullah, Karen L. Butler-Purry
Electrical & Computer Eng. Dept. Texas A&M University
{irfan, klbutler}@tamu.edu

Harsha Nagarajan
Los Alamos National Laboratory (LANL)
harsha@lanl.gov

***Abstract*— This paper presents a two-stage robust optimization framework for maximal load delivery under load uncertainty, implemented in PowerModelsONM.jl and tested on a modified Iowa 240-node system. A cutting-plane master–subproblem process ensures feasibility across all uncertainty realizations, while a scenario-indexed embedded model validates the decisions. Modeling uncertainty at the load-block level improves tractability and preserves consistent, robust restoration performance.**

Keywords—PowerModelsONM (ONM), Maximal Load Delivery (MLD), Robust Optimization, Uncertainty, Microgrids.

I. Introduction

Modern distribution networks face increasing stress from weather events, aging assets, and DER variability. Microgrids improve resilience, but ensuring feasible and optimal operation of large, unbalanced feeders under uncertainty remains challenging. These challenges motivate scalable robust optimization tools for complex network behavior.

Deterministic models use mixed-integer formulations for nominal conditions [1], [2], while stochastic approaches handle uncertainty via scenarios but face scalability issues [3]. Robust optimization ensures feasibility under all realizations within a defined uncertainty set and has been applied to network reconfiguration and microgrid formation [4], [5]. Decomposition-based methods have further improved tractability for large systems [6], [7]. However, most robust optimization frameworks have not been evaluated on large, unbalanced distribution feeders. For instance, [8] considers balanced networks and small systems. While the framework in [9] addresses two stage robust partitioning, it was only evaluated on a small test system (e.g., a 37-bus system) and faced significant computational scalability challenges when the number of uncertain loads were increased.

These shortcomings in [9] motivate this work, which develops and validates a scalable two-stage robust optimization framework for large-scale, three-phase unbalanced distribution systems within PowerModelsONM.jl [10]. The formulation is evaluated on a modified Iowa 240-node system using a scenario-indexed embedded model, multiple uncertainty levels, and load-block based uncertainty modeling to reduce computational complexity while preserving realistic system behavior and demonstrating scalability and consistency of the robust optimization method.

The key contributions of this paper are as follows. (1) The two stage robust optimization framework [9] was implemented on a modified 240 node distribution system to evaluate scalability, demonstrating that the approach can scale to large unbalanced feeders with multiple distributed energy resources and hundreds of loads. (2) A scenario-indexed embedded model was developed to validate the two-stage formulation. (3) Load-block based uncertainty modeling was introduced to enlarge the uncertainty space while reducing computational burden through load block-level rather than individual load uncertainty, thereby improving algorithmic convergence. (4) Multiple uncertainty levels were studied to evaluate how load variability affected network partitioning and restoration performance. Together, these contributions advanced scalable robust optimization methodologies for distribution network operation and microgrid formation, demonstrating computational tractability and robustness under extensive uncertainty while supporting resilient restoration planning in large-scale, unbalanced systems.

The remainder of this paper is organized as follows. Section II presents the mathematical formulation of the robust optimization framework. Section III provides details of the implementation and algorithmic approaches. Section IV discusses the case studies and results, and Section V concludes the paper with future research directions.

II. Problem Formulation

A. Two-Stage Optimization *for Individual Load Uncertainty Modeling*

The two-stage robust optimization framework [9] determines the optimal network configuration and distributed energy resource (DER) dispatch that remain feasible under uncertain load realizations. The first-stage (master problem) selects partitioning, switching, and nominal DER setpoints before uncertainty is realized, with an objective that maximizes load restoration and minimizes generation cost while enforcing feasibility through coupling with the subproblem.

The master problem [9] is subject to three main constraints. Radiality constraints ensure loop-free structure during restoration, as described in [11]. Grid-forming inverter constraints define the operational roles of DERs, distinguishing between grid-forming and grid-following units to preserve voltage and frequency stability within each energized island [9]. Finally, feasibility cuts iteratively link the master and subproblem to guarantee that all first-stage decisions remain feasible under admissible uncertainty.

Load uncertainty in equation (1) in [9] is modeled in (S_2) using a bounded polyhedral uncertainty set. However, its

This work was supported in part by the Triad National Security, LLC. The research work conducted at Los Alamos National Laboratory is done under the auspices of the National Nuclear Security Administration of the U.S. Department of Energy under Contract No. 89233218CNA000001
979-8-3315-8138-1

presentation contains typographical inconsistencies. Equation (1) below provides a corrected and consistent form of the uncertainty set, which is adopted in this work to model load uncertainty within the robust optimization framework.

$$\mathcal{U} = \left\{ u_d^{\phi} \in \mathbb{R}^{|\mathcal{D}\times\Phi|} \mid u_d^{\phi} = \zeta_d^{+} \left(\overline{s}_d^{\phi} - s_{0,d}^{\phi} \right) - \zeta_d^{-} \left(s_{0,d}^{\phi} - \underline{s}_d^{\phi} \right),\ \forall d \in \mathcal{D},\ \phi \in \Phi_d \right\} \tag{1}$$

where u_d^{ϕ} represents the deviation of load $d \in \mathcal{D}$ on phase $\phi \in \Phi_d$, and "|" denotes "such that". $\mathcal{U}$ denotes the uncertainty set of admissible load deviations. $s_{0,d}^{\phi}$ is the nominal load, $\overline{s}_d^{\phi}$, $\underline{s}_d^{\phi}$ are the upper and lower bounds of the uncertain load, respectively. ζ_d^{+}, ζ_d^{-} represent the direction of uncertainty.

The subproblem [9] represents the second stage of the two-stage robust optimization framework, where the first-stage decisions are fixed, and the model determines the worst-case load realization and corresponding operational response. The subproblem is formulated as a bilevel max–min problem: the outer maximization identifies the worst-case load deviations, while the inner minimization computes the optimal corrective actions minimizing operational cost. Equation (2) revised the inner minimization objective of (E) in [9] by replacing the term o_g^{ϕ} with $o_g^{(+\phi)} + o_g^{(-\phi)}$, ensuring accurate representation of generator ramping adjustments under uncertainty. Equation (3) revised power balance constraint in problem (E) of [9], based on the uncertainty set defined in (1) in this work. The max-min problem is subjected to power flow constraints and the generator constraints in equations (18b) -(18g) in [9]. The revised equation (2) and (3) are shown below.

$$\max_{u\in\mathcal{U}} \min_{h^{+},h^{-},o^{+},o^{-}} \left[\omega \left(\sum_{i\in\mathcal{N}} \sum_{\phi\in\Phi_i} \left(h_i^{+,\phi} + h_i^{-,\phi} \right) \right) + \sum_{g\in\mathcal{G}} \sum_{\phi\in\Phi_g} c_{1,g} \left(o_g^{+\phi} + o_g^{-\phi} \right) \right] \tag{2}$$

$$\sum_{ij\in\mathcal{E}_i} s_{ij}^{\phi} + h_i^{+,\phi} - h_i^{-,\phi} = \sum_{g\in\mathcal{G}_i} \left(\left(s_g^{\phi^*} + o_g^{+,\phi} - o_g^{-,\phi} \right) - z_i^{*} \sum_{d\in\mathcal{D}_i} \left(s_{0,d}^{\phi} + \zeta_d^{+} \left(\overline{s}_d^{\phi} - s_{0,d}^{\phi} \right) - \zeta_d^{-} \left(s_{0,d}^{\phi} - \underline{s}_d^{\phi} \right) \right) - \sum_{c\in\Phi_i} y_c^{\phi} w_i^{\phi} \right) \tag{3}$$

where $h_i^{+,\phi}, h_i^{-,\phi}$ are slack variables that capture imbalance violations in active and reactive power at node i on phase ϕ.

B. Two-Stage Optimization for Load-Block Based Uncertainty Modeling

The two-stage cutting-plane algorithm for individual loads can become computationally intensive since the subproblem is solved for each uncertain load. As the number of uncertain loads increases, the total number of uncertainty realizations grows exponentially, reaching up to $2^{|D|}$ possible combinations, resulting in significant computational overhead and limited scalability for large-scale networks.

To address this challenge, the cutting-plane algorithm described in III-A is extended to incorporate load block-based uncertainty modeling using the redefined equations. The Maximum Load Delivery (MLD) formulation [10] already groups load connected via non-switchable nodes into load blocks, where all loads within a load block are either fully energized or fully de-energized. Building on this structure, uncertainty is associated with each load block $b \in B$, allowing the uncertain loads $d \in D_b$ within that load block to deviate collectively in one direction. This provides flexibility to model either all loads or only a subset of loads within each load block as uncertain, depending on the desired level of uncertainty. To formally capture the worst-case scenarios, we define the uncertainty set $\mathcal{U}$ using a budget-constrained approach. Intuitively, this limits the total number of load blocks that can deviate from their nominal values simultaneously, preventing overly conservative solutions.

To address that limitation, equations (1) and (3) are reformulated in equations (4) and (5) to represent load block-level uncertainty, where each block $b \in \mathcal{B}$ may contain multiple uncertain loads $d \in \mathcal{D}_b$ within that load block. Here, b denotes an *uncertain block*, and $\mathcal{D}_b \subseteq \mathcal{L}_b$ represents the subset of uncertain loads associated with block b , where $\mathcal{L}_b$ is the complete set of loads within that load block. The number of uncertain loads in a load block satisfies $|\mathcal{D}_b| \leq |\mathcal{L}_b|$, ensuring flexibility between fully uncertain blocks, where all loads within a load block are uncertain ($|\mathcal{D}_b| = |\mathcal{L}_b|$), and partially uncertain load blocks, where only a subset of loads are uncertain ($\mathcal{D}_b \subset \mathcal{L}_b$).

$$u_{b,d}^{\phi} = \zeta_b^{+} \left(\bar{s}_{b,d}^{\phi} - s_{0,b,d}^{\phi} \right) - \zeta_b^{-} \left(s_{0,b,d}^{\phi} - \underline{s}_{b,d}^{\phi} \right) \tag{4}$$

$$\sum_{ij\in\mathcal{E}_i} s_{ij}^{\phi} + h_i^{+,\phi} - h_i^{-,\phi} = \sum_{g\in\mathcal{G}_i} \left(\left(s_g^{\phi^*} + o_g^{+,\phi} - o_g^{-,\phi} \right) - z_i^{*} \sum_{d\in\mathcal{D}_i} \left(s_{0,b,d}^{\phi} + \zeta_b^{+} \left(\bar{s}_{b,d}^{\phi} - s_{0,b,d}^{\phi} \right) - \zeta_b^{-} \left(s_{0,b,d}^{\phi} - \underline{s}_{b,d}^{\phi} \right), \forall \right) - \sum_{c\in\Phi_i} y_c^{\phi} w_i^{\phi} \right) \quad \forall b \in \mathcal{B}, d \in \mathcal{D}_b \tag{5}$$

where $u_{b,d}^{\phi}$ denotes the uncertain load d in block b , $s_{(0,b,d)}^{\phi}$ denotes the nominal active or reactive power, and $\bar{s}_{(b,d)}^{\phi}$ and $\underline{s}_{(b,d)}^{\phi}$ are its upper and lower bounds, respectively. The binary variables ζ_b^{+} and ζ_b^{-} indicate the direction of uncertainty at the block level, determining whether the uncertain loads within that block will take their maximum or minimum deviation.

By defining uncertainty within load blocks, the computational burden of the two-stage cutting-plane algorithm is substantially reduced because the number of subproblems decreases from $2^{|\mathcal{D}|}$ to $2^{|\mathcal{B}|}$. This maintains a realistic and scalable representation of uncertain load variations while significantly improving computational tractability.

III. Implementation

A. Cutting Plane Algorithm for Individual Load and Load-Block Based Uncertainty Modeling

The revised Algorithm 1, adapted from [9], iteratively coordinated between the master and subproblems to achieve a robust and feasible network configuration. This algorithm was used for implementing II(A) and II(B). (S1) The algorithm began with initialization, where the iteration counter, tolerances, and system data were defined. (S2) A warm-start phase was introduced, in which the master problem was solved to obtain an initial configuration including switch states, block energization, and nominal DER setpoints. (S3) Once the first-stage decisions were fixed, the subproblem was solved to determine the worst-case load realization, and the corresponding max–min problem described in II was evaluated under worst-case uncertainty. (S4) If the power imbalance variables h^+ and h^- exceeded the specified tolerance, a feasibility cut was generated using the dual multipliers from the subproblem and appended to the master problem. (S5) The iteration counter was updated, and the master problem was re-solved with all accumulated cuts until convergence was achieved. (S6) Upon termination, the algorithm generated the final robust configuration $x^*$and generator adjustment variables $o^+$and o^-, representing the positive and negative deviations in generator outputs under the worst-case realization. The key revisions from [9] included the introduction of a warm-start initialization and the replacement of steps 5 and 6 through the revised max–min problem described in Section II.

B. Scenario-Indexed Embedded Model

A scenario-indexed embedded model was implemented to validate the two-stage robust optimization framework. The subproblem was integrated directly into the master problem, forming a single-level optimization model. Each possible load uncertainty realization was represented as a distinct scenario, with a complete set of subproblem (E) constraints embedded for each scenario index, and the objectives of (E) and (M) were combined into a unified formulation. Mathematically, the model replicated the subproblem structure for every enumerated combination of binary uncertainty variables (ζ^+, ζ^-), such that all $2^{|U|}$extreme points of the uncertainty set were represented simultaneously within the master problem.

The first-stage decision variables, such as switch statuses, block energization indicators, and nominal DER setpoints, were shared across all scenarios to maintain a common configuration. In contrast, the operational variables used in the subproblem, such as generator ramp and power flow variables, were defined separately for each scenario. This formulation eliminated iterative cut generation by enforcing feasibility across all uncertainty realizations within a single optimization model. Although this embedded approach increased computational size compared to the cutting-plane method, it provided a unified benchmark to validate the two-stage framework. The model was implemented in PowerModelsONM.jl to validate the two-stage formulation of section III-A by comparing switching, generation, and load energization between both models.

IV. Case Studies and Results

The optimization studies were performed on a workstation equipped with an Intel Core i9-14900K processor (3.2 GHz) and 64 GB of RAM, using the Julia programming language (v1.12) integrated with JuMP (v1.23.5) for model formulation and optimization. The PowerModelsONM.jl package (v4.0.0) was utilized for model development, with the LinDist3Flow formulation applied for the two stage robust Optimization. Gurobi (v12.0.3) served as the optimization solver, while OpenDSS was used for system simulation and preprocessing of network data, which were subsequently imported into the ONM framework for analysis.

A. Modified Iowa 240 Node System

This study uses a modified version of the Iowa State 240-bus unbalanced distribution system supported by one year of smart meter data. Several enhancements introduced in [10] were adopted, including the replacement of single-phase split transformers with their high-side equivalents for simplified modeling. Also, 4 PVs, 3 BESS, and I DG were integrated into existing network partitions to form microgrids, and three tie-switches were added to enable network reconfiguration. In this work, three system configurations were analyzed for three different case studies.

Case 1 follows the modifications presented in [10] and uses the base model at a single time step without any energy storage units. Case 2a builds on this configuration [10] by placing one PV unit and one diesel generator at the same nodes on each feeder, providing distributed energy resource support across all microgrids. The network layout follows the single-line diagram in [12], which includes the additional switches. In Case 2b and Case 3, the BESS units shown in [12] are removed, and the PV and diesel generators introduced in Case 2a are retained at the same nodes as shown in fig 1. In Fig 1, nodes are represented as dots, the substation as a bar, switchable lines as squares, and block with blue square with numbers. The final model contains 4 DGs, 4 PVs and 192 loads, and in all cases the grid remains disconnected at switches 101, 102, and 103.

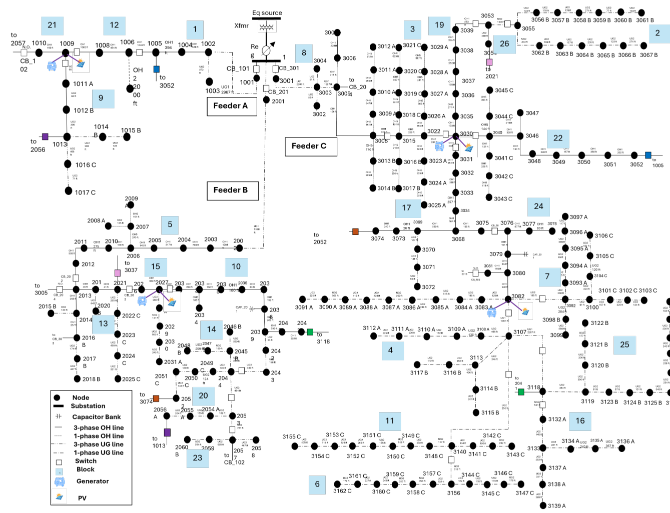

Fig 1. Modified Iowa 240 Node system.

B. Case Studies and Analysis

1) Case 1: Scenario-Indexed Embedded Model Validation

In Case 1, the proposed two-stage optimization framework was validated using two representative loads (1015 and 2017) to ensure computational simplicity.The results from the Cutting Plane Algorithm (Section III-A) for II(A) and the Scenario-Indexed Embedded Model (Section III-B) were compared to verify the consistency of the optimal set points. Fig. 2 illustrated the outcomes of Case 1.As shown in Fig. 2, PV1 and PV3 produced identical active power in both formulations. PV2 showed no generation on phase B in III-B, similar to PV4 in III-A, while on phases A and C, PV2 in III-A generates slightly higher power. In contrast, PV4 and Gen3 exhibited marginally higher output on phases A and C, respectively, in III-B. Despite these minor per-phase differences, the total power generation across all units was equivalent, as lower values in one phase were balanced by higher values in phases. The network configuration was the same in both cases, with Feeder A

979-8-3315-8138-1

connected to Feeder B through switch 102 and Feeder B connected to Feeder C through switch 303. All loads were restored in both formulations, confirming equivalent restoration performance between III-A and III-B.

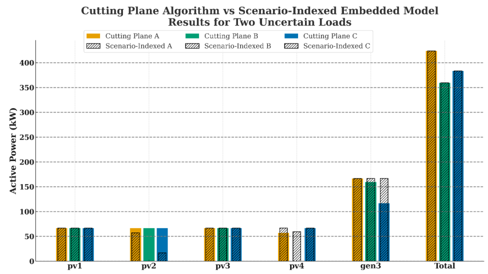

Fig 2. Comparison of Cutting plan Algorithm with the Scenario-indexed Embedded Model Results.

2) *Case2: Cutting-Plane Algorithm for Varying Levels of Individual Load Uncertainty*

Case 2.1 analyzed the performance of the Cutting-Plane Algorithm (Section III-A for IIA) on the modified 240-node system described in [12], which incorporated additional generators and removed batteries to improve flexibility. Feeder A included Gen1 (50 kW, PF 0.8) and PV1 (50 kW, PF 1.0); Feeder B3 included Gen2 (200 kW, PF 0.8) and PV2 (70 kW, PF 1.0); Feeder C1 included Gen3 (300 kW, PF 0.8) and PV3 (50 kW, PF 1.0); Feeder C2 included Gen4 (500 kW, PF 0.8) and PV4 (100 kW, PF 1.0). The system was evaluated under uncertainty levels of 10%, 30%, 60%, and 90% using incrementally increasing uncertian load to nine. The microgrids were labeled from 1 to 4, each corresponding to distinct feeder sections: (A) nodes 1001 to 1017, (B1) nodes 2001 to 2012, (B2) nodes 2013 to 2025, (B3) nodes 2026 to 2060, (C1) nodes 3001 to 3075, and (C2) nodes 3076 to 3162, as shown in Fig. 3

At 10% uncertainty, the system formed three microgrids: MG1 (A), MG2 (B3), and MG3 (B1 + B2 + C). All loads were restored, and generator ramping remained minimal, with Gen3 showing the highest ramping (≈5.5%) while others remained below 1%. At 30% uncertainty, the system reconfigured into four microgrids: MG1 (A), MG2 (B3), MG3 (B1), and MG4 (B2 + C1 + C2). Seven loads (nodes 2002-2011) were not restored. Gen3 provided most flexibility (≈12.4%), followed by Gen4 (≈4.9%), while Gen1 and Gen2 remained below 1%.

At 60% uncertainty, two microgrids were formed: MG1 (A + B2 + B3 + C1 + C2) and MG2 (B1). Seven loads (2002–2011) remained unserved, but the system maintained stable operation through coordinated support among feeders. Generator ramping increased, with Gen2 (≈13.5%), Gen3 (≈6.9%), Gen4 (≈4%), and Gen1 (≈1%) providing system balance. This demonstrated that coordinated redispatch of local generation enabled the network to remain stable even when some loads could not be fully restored. At 90% uncertainty, three microgrids were formed: MG1 (A), MG2 (B3, not restored), and MG3 (B1 + B2 + C1 + C2). MG2 remained deenergized as restoring it would exceed the 30% generator ramp limit. Gen3 provided the primary flexibility (≈14%), followed by Gen4 (≈4%) and Gen1 (≈1%). Loads in MG1 and MG3 operated near their lower uncertainty bounds to maintain feasibility, while coordination between Feeders B and C sustained stable and secure system operation. These results demonstrated that coordinated redispatch of local generation enabled the network to remain stable even when some loads cannot be fully restored.

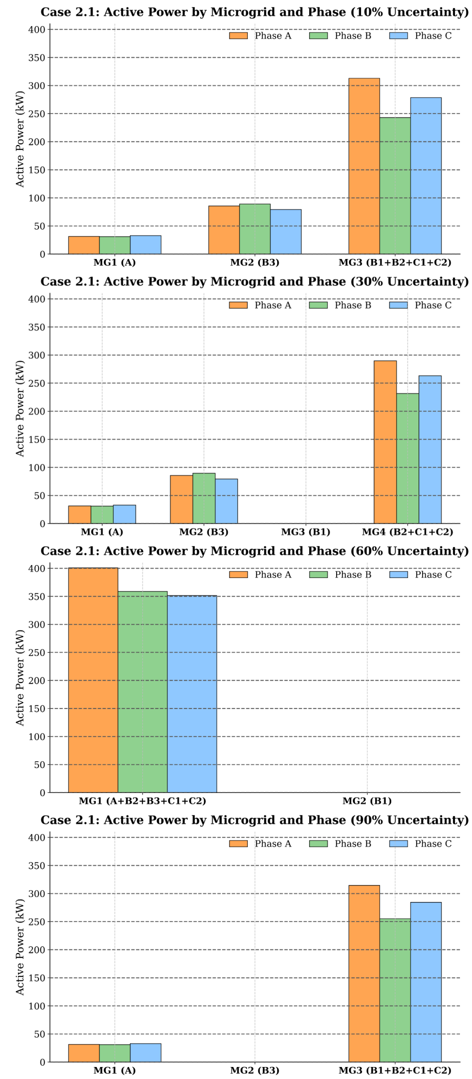

Fig 3. Active power by microgrid and phase for Case 2.1 at four uncertainty levels (10%, 30%, 60%, 90%)

Case 2.2 examined the performance of the Cutting-Plane Algorithm on the modified Iowa 240-node distribution system, based on the configuration in Case 2.1. Additional line and tie switches [12] were included to improve reconfiguration flexibility and enable multiple restoration pathways. The system is divided into microgrids, as shown in Fig. 4 with feeder sections (A) 1001-1017, (B1) 2001-2012, (B2) 2013-2025, (B3) 2026-2043, (B4) 2044-2052, (B5) 2053-2060, (C1) 3001-3075, and (C2) 3076-3162.

At 10% uncertainty, the results were similar to Case 2.1, with Microgrid 2 including blocks B3-B5. At 30% uncertainty, all feeder sections merged into a single microgrid. All loads were restored, unlike in Case 2.1 where seven loads remained unserved. The added switches improved power transfer between feeders, allowing generators to ramp within their 30% limits: Gen1 (≈21%), Gen2 (≈22%), and Gen4 (≈6%).

At 60% and 90% uncertainty, the system exhibited the same configuration and total MG power generation but with different

979-8-3315-8138-1

ramping patterns. The system formed two microgrids: MG1 (all feeders except B4) and MG2 (B4 de-energized), leaving eight loads unrestored. Most uncertain loads operated at their upper bounds. At 60%, Gen3 ramped about 24%, while Gen1 and Gen2 ramped 9% and 1%, respectively. At 90%, Gen1 and Gen2 become dominant with 26% ramping, and Gen3 reduces to 19%. Unlike Case 2.1, where limited switching prevented full restoration of block B3, the additional switches in Case 2.2 subdivided B3 into B3-B5, allowing MLD to isolate only B4 rather than de-energizing the entire B3 section.

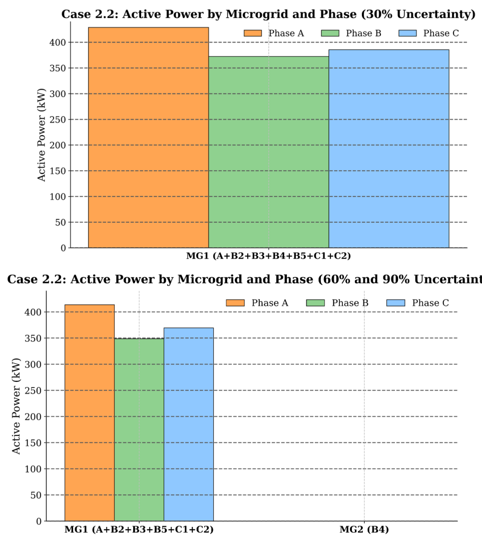

Fig 4. Active power by microgrid and phase for Case 2.2 at three uncertainty levels (30%, 60%, 90%)

3) Case 3: Cutting-Plane Algorithm for Load-Block Based Uncertainty

Case 3 corresponded to the implementation described in Section IIIA for II-B where load uncertainty was modeled at the load block level, and the subproblem was modified to reflect this load block-based representation.

In this implementation, nine load blocks (1, 5, 6, 7, 8, 11, 13, 14, and 20) were modeled as uncertain, using the block numbers defined by the ONM during the optimization process. Each block satisfied $|D_b| \leq |L_b|$, allowing flexible representation of partial or full uncertainty. For example, load block 1 in Feeder A included three loads (1003-1005), of which only two loads (1004 and 1005) were uncertain, satisfying $|\mathcal{D}_b| \leq |\mathcal{L}_b|$, while the remaining load blocks included all loads as uncertain ($|D_b| = |L_b|$). In Feeder B, load block 5 included loads 2002–2012, load block 13 included loads 2013-2025, load block 14 included loads 2044-2052, and load block 20 included loads 2053-2056. In Feeder C, load block 8 contained loads 3001–3014, load block 7 included loads 3092–3106, load block 11 contained loads 3140–3143 and 3148–3155, and load block 6 included loads 3144–3162.

Together, these nine load blocks represented 75 uncertain loads while reducing the number of subproblems from 2^{75}in load-level modeling (Case 2) to 2^9, thereby achieving a scalable and computationally efficient implementation of the two-stage robust optimization framework. Case 2 required 2460 s with 19 iterations, whereas Case 3 reduced the runtime to 2160 s with 18 iterations, demonstrating that block-level uncertainty preserves comparable computational effort while avoiding the intractability of 2^{75} realizations. This highlights the tractability advantage of the load-block formulation, reducing the uncertainty set dimensionality from$2^{|\mathcal{D}|}$ to $2^{|\mathcal{B}|}$.

V. Conclusions

This work presents a two-stage robust optimization framework for maximal load delivery in large-scale unbalanced distribution systems, implemented in PowerModelsONM.jl. A key advantage of the proposed load-block formulation is its computational tractability, reducing the uncertainty set dimensionality from $2^{|\mathcal{D}|}$ to $2^{|\mathcal{B}|}$. This enables robust restoration for large networks that would be computationally prohibitive with individual load-level approaches. Validation on a modified Iowa 240-node system confirms that the framework ensures feasible operation across multiple uncertainty levels without compromising solution quality.

Future work will study sensitivity to uncertainty-set design including block definitions and uncertainty bounds, and extend the framework to correlated and time-coupled load uncertainty within multi-step restoration formulations.

VI. Acknowledgment

The authors acknowledge Dr. Russell Bent and Dr. Art Barnes of Los Alamos National Laboratory for their guidance and technical feedback.

VII. References

[1] Z. Li, M. Shahidehpour, F. Aminifar, A. Alabdulwahab, and Y. Al-Turki, “Networked Microgrids for Enhancing the Power System Resilience,” Proceedings of the IEEE, vol. 105, no. 7, pp. 1289–1310, Jul. 2017.
[2] A. Barnes, H. Nagarajan, E. Yamangil, R. Bent, and S. Backhaus, “Resilient Design of Large-Scale Distribution Feeders with Networked Microgrids,” Electric Power Systems Research, vol. 171, pp. 150–157, Jun. 2019.
[3] L. A. Roald, D. Pozo, A. Papavasiliou, D. K. Molzahn, J. Kazempour, and A. J. Conejo, “Power Systems Optimization Under Uncertainty: A Review of Methods and Applications,” Electric Power Systems Research, vol. 214, p. 108725, Jan. 2023.
[4] R. Zhang, K. Qu, C. Zhao, and W. Huang, “Robust Distribution Network Reconfiguration Using Mapping-Based Column-and-Constraint Generation,” arXiv preprint arXiv:2505.24677, May 2025.
[5] Jokar H. Robust optimization for operational management of microgrids integrated with energy hubs and hydrogen refueling stations. International Journal of Hydrogen Energy. 2025 Jun 6;135:295-315.
[6] B. Zeng and L. Zhao, “Solving Two-Stage Robust Optimization Problems Using a Column-and-Constraint Generation Method,” Operations Research Letters, vol. 41, no. 5, pp. 457–461, Sep. 2013.
[7] G. Liu, T. Ollis, N. Stenvig, Y. Xu, Y. Zhang and K. Tomsovic, "Robust Scheduling of Microgrids With Resiliency Constraints," 2019 IEEE Power & Energy Society General Meeting (PESGM), Atlanta, GA, USA, 2019, pp. 1-5,
[8] M. Y. Mahdavi, K. E. K. Schmitt, and F. Jurado, “Robust Distribution Network Reconfiguration in the Presence of Distributed Generation Under Uncertainty in Demand and Load Variations,” IEEE Transactions on Power Delivery, vol. 38, no. 5, pp. 3480–3495, May 2023.
[9] H. Moring, H. Nagarajan, K. Girigoudar, D. M. Fobes, and J. L. Mathieu, “Robust Partitioning and Operation for Maximal Uncertain-Load Delivery in Distribution Grids,” Electric Power Systems Research, vol. 235, Oct. 2024.
[10] D. M. Fobes and R. Bent, PowerModelsONM.jl. [Online]. Available: https://github.com/lanl-ansi/PowerModelsONM.jl, Accessed: May 30, 2025.
[11] S. Lei, C. Chen, Y. Song, and Y. Hou, “Radiality Constraints for Resilient Reconfiguration of Distribution Systems: Formulation and Application to Microgrid Formation,” IEEE Transactions on Power Systems, vol. 35, no. 6, pp. 4529–4540, Nov. 2020.

979-8-3315-8138-1